Monthly Notices
of the
ROYAL ASTRONOMICAL SOCIETY

MNRAS **466,** 3973–3988 (2017)
Advance Access publication 2016 December 24

doi:10.1093/mnras/stw3352

Collisional parameters of planetesimal belts, precursor of debris discs, perturbed by a nearby giant planet

F. Marzari[1]★ and A. Dell'Oro[2]

[1]*Department of Physics, University of Padova, I-35131 Padova, Italy*
[2]*INAF, Osservatorio Astrofisico di Arcetri, Largo E. Fermi 5, I-50125 Firenze, Italy*

Accepted 2016 December 21. Received 2016 December 16; in original form 2016 June 26

ABSTRACT

Planetesimal belts are invoked to explain the prolonged existence of debris discs. Important parameters to model their collisional evolution and to compute the dust production rate are the intrinsic probability of collision P_i and the mean impact velocity U_c. If a planet orbits close to the belt, the values of both these parameters are affected by its secular perturbations yielding a strong correlation between eccentricity e and pericentre longitude ϖ. We adopt a new algorithm to compute both P_i and U_c in the presence of various levels of secular correlation due to different ratios between proper and forced eccentricity. We tested this algorithm in a standard case with a Jupiter-sized planet orbiting inside a putative planetesimal belt finding that it is less collisionally active compared to a self-stirred belt because of the e–ϖ coupling. The eccentricity of the planet is an important parameter in determining the amount of dust production since the erosion rate is 10 times faster when the planet eccentricity increases from 0.1 to 0.6. Also the initial conditions of the belt (either warm or cold) and its average inclination strongly affect P_i and U_c and then its long-term collisional evolution in the presence of the planet. We finally apply our method to the planetesimal belts supposedly refilling the dust discs around HD 38529 and ϵ Eridani. In the most collisionally active configurations, only a small fraction of bodies smaller than 100 km are expected to be fragmented over a time-span of 4 Gyr.

Key words: planets and satellites: dynamical evolution and stability – planet–disc interactions.

1 INTRODUCTION

Debris discs, mostly detected in thermal infrared, are observed around 10–20 per cent of solar-type stars (Hillenbrand et al. 2008; Trilling et al. 2008; Sibthorpe et al. 2013). The micron-sized grains populating these discs are short-lived mostly because of radiation-related forces and collisional erosion. As a consequence, their refilling requires the presence of a reservoir of planetesimals whose collisions constantly produce new dusty debris. Indeed, debris discs are the only signature of these belts whose properties like size distribution, mechanical strength and dynamical excitation cannot be constrained by observations. The only way to link planetesimals and dust is through numerical models reproducing the Spectral Energy Distribution and resolved images of debris discs. However, these models not always give unique solutions.

Analogues of the Solar system asteroid or Kuiper belt, planetesimal belts are leftovers from the planet formation process and they eventually continue to evolve under mutual collisions. The frequency of debris discs as well as the infrared excess strength declines with the stellar age (Krivov 2010) suggesting that the collisional process slowly grinds down the initial planetesimal population. Different mechanisms have been invoked to stir up a planetesimal swarm igniting mutual destructive collisions like self-stirring by larger planetesimals (Chambers & Wetherill 2001; Kenyon & Bromley 2004) and perturbations by planets (Mustill & Wyatt 2009). Concerning this last mechanism, it is still controversial from an observational point of view if there is any significant correlation between stars with dust emission and the presence of known planets (Moro-Martín et al. 2007a; Bryden et al. 2009) even if some of such systems are already known like that in ϵ Eridani (Benedict et al. 2006), Fomalhaut (Kalas et al. 2008) and HD 38529 (Moro-Martín et al. 2007b). From a theoretical point of view, it is expected that debris discs and planets coexist in a large number of systems being both the outcome of dust coagulation and planetesimal accumulation even if debris discs appear to be more common than massive planets (Moro-Martín et al. 2007a). This may be due to the presence of debris discs even in systems where the planetesimals were not able to form the core of giant planets. In this scenario, the dust would be produced in mutual collisions possibly triggered by self-stirring. There are significant observational problems in statistically assessing the probability of finding giant planets and debris

★ E-mail: marzari@pd.infn.it

discs coexisting in the same system. Young stars have a higher percentage of debris discs but radial velocity surveys for planets around them are difficult because of the noise due to stellar activity. On the other hand, planets can be easily detected around old stars where debris discs may have been eroded away by collisional evolution and are expected to be less common. It is also difficult to precisely locate the debris belts in radial distance in order to assess the potential detectability of close-by planets. Finally, it should be noted that the inventory of giant exoplanets is still poor for semimajor axes larger than a few au.

Assuming that in some systems different dynamical mechanisms lead to a configuration with a massive planet in an inside orbit with respect to a debris disc, this would be a particularly interesting architecture since the disc structure is very sensitive to the planet gravitational perturbations potentially driving the formation of arcs, gaps, warps and asymmetric clumps in the disc (Moro-Martín, Wolf & Malhotra 2005; Moro-Martín et al. 2007b). Even the gap between two components debris discs is suspected to be carved by intervening planets scattering away the remnant planetesimals (Su & Rieke 2014; Shannon et al. 2016) and a survey based on direct imaging is searching for planets in systems with double debris discs (Meshkat et al. 2015). In addition to these direct effects, a planet also perturbs the planetesimal belt stirring up their orbits and affecting the collision probability and impact velocity (Mustill & Wyatt 2009). The level of stirring depends on the planet mass, vicinity to the belt, either inside or outside, and orbital eccentricity. An excited planetesimal belt may give origin to a brighter debris disc at start (Wyatt et al. 2007), but its lifetime will be significantly shorter due to the collisional erosion.

We can envisage different scenarios related to the coexistence of planets and debris discs. A single giant planet, which had a limited amount of inward migration, can clear part of the leftover planetesimal population leaving an inner cavity in the planetesimal disc. In this case, we would find a low-eccentricity planet secularly perturbing an external planetesimal belt. This configuration does not exclude the presence of additional planets in the system moving in inside orbits. More complex dynamical configurations are expected when a multi-planet system undergoes a period of extended chaotic evolution characterized by planet–planet scattering. In extreme cases, this dynamical evolution may lead to a complete clearing of local planetesimal belts because of the intense perturbations of the planets on highly eccentric orbits (Bonsor, Raymond & Augereau 2013; Marzari 2014). However, less violent evolutions may lead to a final architecture where a giant planet on an eccentric orbit is located inside, or outside, the surviving belt and it affects its evolution via secular perturbations. The two different mechanisms may lead to a wide range of possible eccentricities for the planet perturbing the belt.

When a planetesimal belt is accompanied by a close-by planet, the relative impact velocity and frequency of collisions of the perturbed belt, used to predict its long-term collisional evolution, cannot be calculated with the Öpik/Wetherill analytic formulation (Öpik 1951; Wetherill 1967) even in the improved formulations developed to study the evolution of the asteroid belt (see Davis et al. 2002 for a review). In the presence of a massive planet, in particular if on a highly eccentric orbit, the forced component in the secular evolution of the planetesimal orbits may lead to a strong correlation between eccentricity and perihelion longitude. This correlation invalidates the Öpik/Wetherill methods based on a uniform distribution of the orbital angles (perihelion longitude and node longitude) derived under the assumption of periodic circulation of the two angles. These methods work properly when describing the evolution of the asteroid or Kuiper belt in the Solar system where the forced eccentricity is significantly smaller than the proper one, but in dynamical configurations where the planetesimal ring is perturbed by a giant planet on a highly eccentric orbit they fail.

A first attempt to overcome this problem is described in Mustill & Wyatt (2009) where they first derive refined values of the forced eccentricity from which they compute an average value of the impact velocity between the planetesimals multiplying the forced eccentricity by the local Keplerian velocity and a constant value $c \sim 1.4$. In this paper, we apply an innovative semi-analytic method to estimate both the intrinsic probability of collision P_i, i.e. the collision rate per unit cross-section area of target and projectile per unit time, and the average collision speed U_c, derived from a detailed statistical frequency distribution of the relative velocities, in a planetesimal belt perturbed by an eccentric giant planet. This method is designed in order to fully account for the different levels of correlation between eccentricity and perihelion longitude of the planetesimals caused by the secular dynamics. Both P_i and U_c are needed to properly model the collisional evolution of a planetesimal disc and predict the dust production rate refilling the related debris disc. In particular, P_i is more relevant in establishing the amount of erosion of the belt. We consider two distinct plausible scenarios where, prior to the evolution of the perturbing planet close to the belt, the planetesimal disc was either dynamically non-excited (cold population) or excited (warm population). In the former case (cold population), when the planet approaches the belt during its evolution, the proper eccentricity of the planetesimals is immediately excited to a value approximately equal to the secular forced one (Thébault, Marzari & Scholl 2006). This is also the scenario explored by Mustill & Wyatt (2009), and it is the dynamical configuration where the correlation between e and ϖ is maximized. If instead the eccentricities of the planetesimal population were already significantly excited when the planet sets in and begins to perturb the belt (warm belt), a different dynamical configuration is achieved where the proper and forced eccentricities may significantly differ. We will consider the cases where the eccentricity, prior to the onset of the secular perturbations, is an increasing fraction of the forced eccentricity. In these cases after the onset of the secular perturbations, the degree of correlation between e and ϖ will be less robust within the belt and pseudo-librator states will appear in the population influencing the values of both P_i and U_c. While modelling a warm belt, it is reasonable to expect that also the inclination is excited as well so we will explore the effect of a high planetesimal inclination on both the collisional parameters.

If a belt is densely populated by planetesimals, a significant collisional damping of the eccentricity may occur (Stewart & Wetherill 1988) leading it to a state of cold belt before the planet approaches. After the planet sets into a perturbing orbit, the collisional damping may still be efficient in reducing the eccentricity, but in this case it will affect only the proper term causing its progressive decrease. We explore also this scenario and estimate the values of the collisional parameters to compare with non-damped cold and warm belts.

In Section 2, we briefly summarize the expected dynamical behaviour of a planetesimal belt perturbed by a planet. In Section 3, we outline the method developed to compute the average values of intrinsic probability of collision P_i and impact velocity U_c for a belt characterized by the above-mentioned secular dynamics. In Section 4, we apply the method to a 'standard' case to illustrate the effects of the secular dynamics and compare the predicted values of U_c with those derived by Mustill & Wyatt (2009). We also derive and compare the values of the collisional parameters in cold and

warm belts with and without inclination excitation. In Section 5, we model the collisional evolution of a putative belt with the previously estimated collisional parameters while in Section 6 we model a real system, HD 38529, and compare its evolution with that of ϵ Eridani. Finally, in Section 7 we summarize and discuss our results.

2 SECULAR EVOLUTION AND CORRELATION BETWEEN ECCENTRICITY AND PERIHELION LONGITUDE

The dynamical evolution of a minor body population perturbed by a planet is classically described by the linear secular theory of Laplace–Lagrange (Murray & Dermott 1999). For a mass-less planetesimal population, the evolution with time of the non-singular variables $h = e \sin\tilde{\omega}$ and $k = e \cos\tilde{\omega}$, where e and $\tilde{\omega}$ are the eccentricity and longitude of the pericentre of the osculating orbit, respectively, is given by

$$h = e_{\rm p} \sin(At + B) + e_{\rm f}$$

$$k = e_{\rm p} \cos(At + B), \quad (1)$$

where B is a constant determined by the initial conditions of the system, $e_{\rm p}$ is termed proper eccentricity while $e_{\rm f}$ is the forced one. In our case, we consider the simplified situation in which the planet is not perturbed by additional bodies so that $e_{\rm f}$ is constant. In equation (1), we assume that the reference frame for the computation of the orbital elements is aligned with the apsidal line of the planet orbit. Approximate values for the proper frequency A and the forced eccentricity $e_{\rm f}$ can be derived from the simplified linear disturbing function (Murray & Dermott 1999) and are given in Mustill & Wyatt (2009)

$$e_{\rm f} \sim \frac{5}{4}\alpha e_{\rm pl}$$

$$A \sim n\frac{3}{4}\frac{m_{\rm pl}}{m_{\rm s}}\alpha^2\bar{\alpha}, \quad (2)$$

where $m_{\rm s}$ is the mass of the central body (the star), $e_{\rm pl}$ is the eccentricity of the planet and n is the mean motion of the test body. For a configuration in which the planet is interior to the planetesimal orbit, $\alpha = \frac{a_{\rm pl}}{a}$ and $\bar{\alpha} = 1$ while $\alpha = \frac{a}{a_{\rm pl}}$ and $\bar{\alpha} = \alpha$ for an exterior planet. a is the semimajor axis of the planetesimal and $a_{\rm pl}$ the semimajor axis of the planet (Murray & Dermott 1999; Mustill & Wyatt 2009). This classical perturbation theory works far from mean motion and secular resonances and, as a consequence, some values of α lead to incorrect predictions. In addition, the theory has been developed to second order in the eccentricity and inclination of the bodies, and it is a good approximation only for small values of these orbital parameters. Among known extrasolar planets, a significant fraction have high orbital eccentricities for which either semi-numerical approaches (Michtchenko & Malhotra 2004) or higher order theories (Libert & Henrard 2005) are preferable. However, a numerical exploration of the reliability of the formulas of the linear theory even for large values of $e_{\rm pl}$ by Mustill & Wyatt (2009) has shown that the precession rate can be well described by the disturbing function developed by Heppenheimer (1978) for binary stars:

$$A \sim 2\pi n\frac{3}{4}\frac{m_{\rm pl}}{m_{\rm s}}\frac{\alpha^2\bar{\alpha}}{4\left(1-e_{\rm pl}^2\right)^{3/2}} \quad (3)$$

for values of $e_{\rm pl}$ beyond 0.2 even if the correction proposed by Thébault et al. (2006) was not tested. This last is a more accurate prescription for the frequency of the secular oscillations induced by a binary companion empirically derived from several numerical simulations. In our context, a very precise value of the frequency A is not strictly required since what matters is that the randomization of the angles is achieved. A constant frequency of circulation is the only assumption about $\theta = At + B$ used in our statistical model. The forced eccentricity $e_{\rm f}$ is instead well approximated by the linear secular theory even for large values of $e_{\rm pl}$.

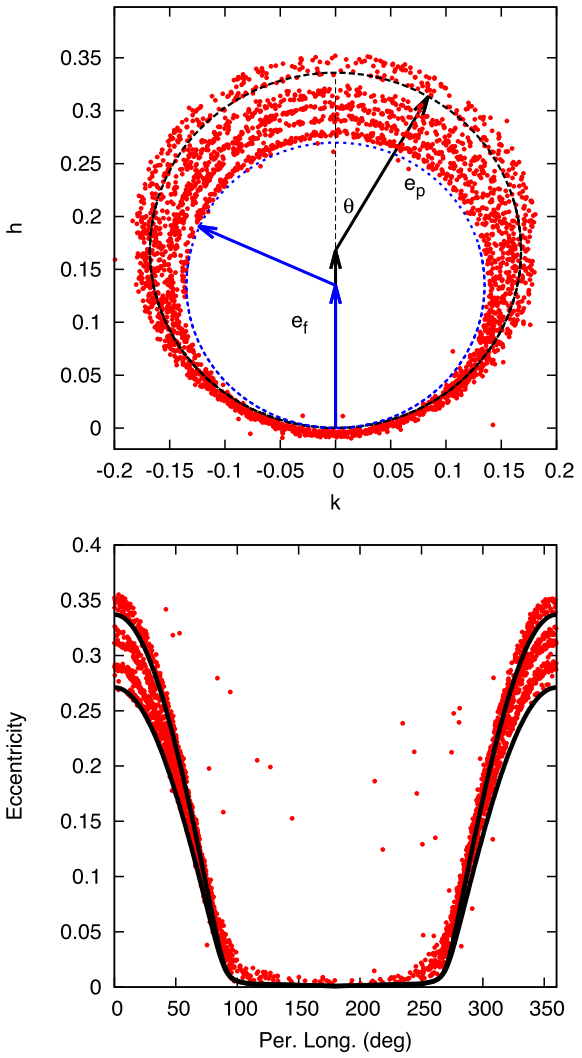

Figure 1. Secular evolution of a population of planetesimals moving in a ring with semimajor axis ranging from 15 to 20 au and initially circular orbits. They are perturbed by a Jupiter-sized planet with $a_{\rm pl} = 5$ au and eccentricity $e_{\rm pl} = 0.5$. In the top panel, the evolution of the non-singular h and k variables is illustrated [$h = e\cos(\varpi)$, $k = e\sin(\varpi)$]. The arrows show the forced $e_{\rm f}$ and proper $e_{\rm p}$ eccentricities for $a = 15$ au (in blue) and $a = 20$ au (in black), which, once combined, give the eccentricity of the planetesimals. The blue and black dashed lines show the curves obtained by combining proper and forced eccentricity. In the bottom panel, the correlation between ϖ and e is highlighted.

To test the reliability of the linear secular theory in dealing with the main dynamical features of a planetesimal belt perturbed by an eccentric planet, we have compared the outcome of a short-term numerical simulation with the predictions of the theory. In Fig. 1, we show the evolution with time of a population of planetesimals orbiting between 15 and 20 au on initially circular orbits and perturbed by a planet at 5 au with an eccentricity $e_{\rm pl} = 0.5$. The 15th-order RADAU integrator (Everhart 1985) has been used for this

short-term simulation. In the upper panel, we show the h and k variables after about 10 Myr of evolution. The pericentre longitude is randomized since the period of the secular circulation is lower than 1 Myr and the integration time-span is also significantly longer than the 'crossing time' defined in Mustill & Wyatt (2009) for an internal perturber. This time is given by

$$t_{\rm cross} \sim 1.53 \times 10^3 \frac{\left(1-e_{\rm pl}^2\right)^{3/2}}{e_{\rm pl}} \left(\frac{a}{10\,{\rm au}}\right)^{\frac{9}{2}} \times \left(\frac{M_*}{{\rm M}_\odot}\right)^{\frac{1}{2}} \times \left(\frac{m_{\rm pl}}{{\rm M}_\odot}\right)^{-1} \times \left(\frac{a_{\rm pl}}{1\,{\rm au}}\right)^{-3} {\rm yr}, \quad (4)$$

and, for our test belt, the longest $t_{\rm cross}$ is about 3.6×10^5 yr.

The theoretical evolution for e and ϖ predicted by the linear secular theory can be derived combining the two vectors drawn in the plot representing the forced $\boldsymbol{e}_{\rm f}$ and proper $\boldsymbol{e}_{\rm p}$ eccentricities. In the bottom panel, the planetesimal eccentricity is shown as a function of the perihelion longitude ϖ and compared to the theoretical curve. The analytic curves are computed for a single value of semimajor axis and, as a consequence, they only match the evolution of the planetesimals with initial semimajor axis similar to that used in the computation of the curves. The agreement between the linear theory and the numerical results is really good apart from a few scattered points that are due to the effects of mean motion resonances with the planet and can be neglected.

In the figures, we have assumed that $e_{\rm p} \sim e_{\rm f}$, condition that is based on the premise that, before being perturbed by the planet, the planetesimals were initially on unperturbed almost circular orbits with $e_{\rm p0} \sim 0$. The approximation $e_{\rm p} \sim e_{\rm f}$ is common when exploring the perturbations of a massive body on an initially cold planetesimal belt (Heppenheimer 1978; Whitmire et al. 1998). In particular, if the planet is injected on a highly eccentric orbit after a period of dynamical instability, the belt of planetesimals will suddenly feel the strong secular perturbations of the planet. If we assume that as 'time 0' of the secular perturbations the belt was cold with $e_{\rm p0} \sim 0$, then the condition $e_{\rm p} \sim e_{\rm f}$ is naturally imposed in the subsequent evolution. We term here $e_{\rm p0}$ the proper eccentricity before the onset of the planet perturbations. In this case, it would not be correct to call it a 'proper' eccentricity since it is just the average eccentricity of the cold belt. However, since it will determine the subsequent value of the proper eccentricity once the planet begins to perturb the belt, hereinafter we will use $e_{\rm p0}$ to indicate it.

A scenario different from that of an initial cold belt is produced by a belt that has been excited before the arrival of the perturbing planet, a warm belt. Various mechanisms may contribute to the dynamical excitation like stellar flybys, self-stirring and planet stirring related to an extended period of planet–planet scattering (see Matthews et al. 2014 for a review). This last mechanism, due to its large variety of possible outcomes, may activate the planetesimal belt inducing high eccentricities and inclinations before a planet is deposited on a finally stable orbit close to the belt (Bonsor et al. 2013; Marzari 2014). In a warm belt, the initial planetesimal eccentricity $e_{\rm p0}$ is significantly higher than 0 at the time of the planet approach. The secular modelling of an initially warm belt is more complex with respect to that of a cold belt since in the former case the initial conditions for the secular evolution are different from the simple assumption $e_{\rm p} \sim e_{\rm f}$. In Fig. 2, we show how the new proper eccentricity $e_{\rm p}$ of each planetesimal in the belt, after the planet perturbations are switched on, can be computed from $e_{\rm p0}$ (initial average eccentricity of the belt before the approach of the planet) and how the secular theory can be used to predict the

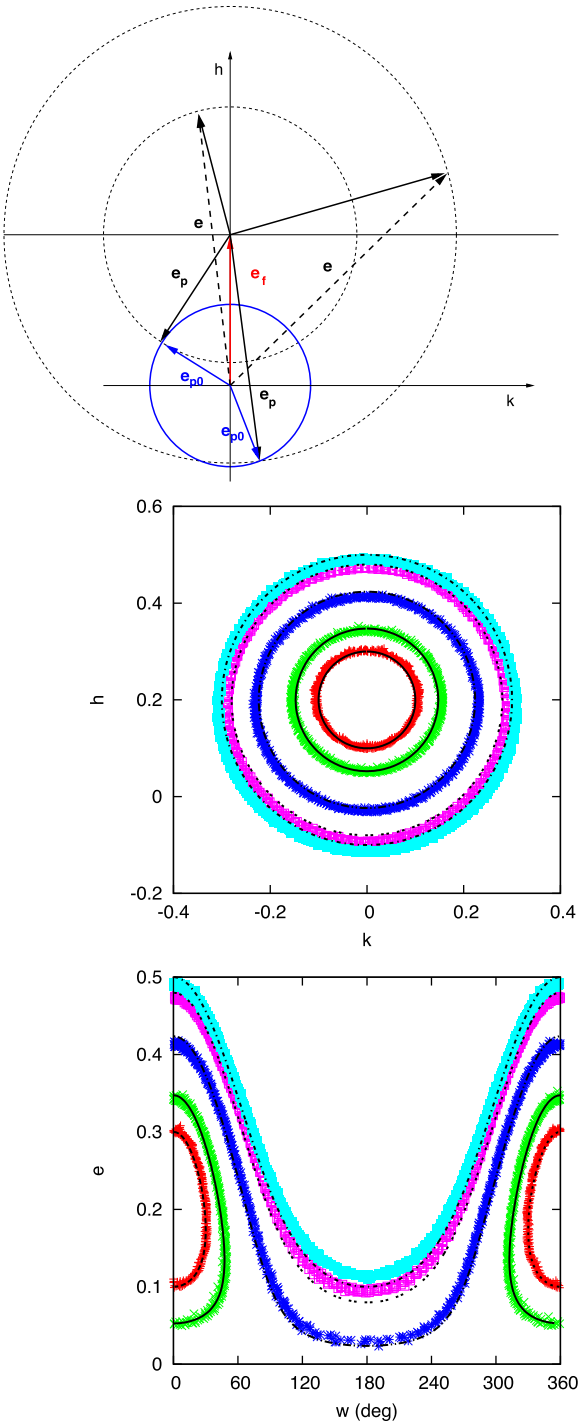

Figure 2. In the upper panel, the secular dynamics is sketched. The blue circle describes the location of the tip of the proper eccentricity vector $\boldsymbol{e}_{\rm p0}$ in an unperturbed warm belt. When the planet perturbs the belt, new initial proper vectors $\boldsymbol{e}_{\rm p}$ are computed joining the tip of $\boldsymbol{e}_{\rm f}$ with the tip of $\boldsymbol{e}_{\rm p0}$. Once the initial $\boldsymbol{e}_{\rm p}$s are computed in this way, the secular evolution can be predicted following the circle centred on the tip of $\boldsymbol{e}_{\rm f}$ and depicted by the tip of $\boldsymbol{e}_{\rm p}$. In the middle and lower panels, the secular behaviour is compared to the outcome of numerical integrations. We select five orbits with semimajor axis equal to 15 au, initial values $e_{\rm p0} = 0.5 \cdot e_{\rm f}$ and five different values of the initial pericentre longitude 0°, 45°, 90°, 135° and 180°. The analytic predictions are given by the dashed continuous lines and they match closely the numerical results drawn by different colours depending on the initial value of ϖ. In both panels, for small values of $e_{\rm p}$, pseudo-librations around 0° are observed (red and green points).

subsequent dynamical evolution. In the upper panel of Fig. 2, we sketch the mode of operation of the secular theory using vector formalism. The blue circle marks the location of the tips of all the initial proper eccentricity vectors $\boldsymbol{e}_{\rm p0}$s of the warm belt. All these vectors have the same modulus (we assume that all planetesimals have the same initial $e_{\rm p0}$ equal to the average of the belt) while their orientation is random depending on ϖ. When the planet begins to perturb the belt, a common forced eccentricity vector $\boldsymbol{e}_{\rm f}$ appears in the secular evolution. As a consequence, each body will acquire a new proper eccentricity vector $\boldsymbol{e}_{\rm p}$ that depends on the initial proper eccentricity vector $\boldsymbol{e}_{\rm p0}$ through the relation $\boldsymbol{e}_{\rm f} + \boldsymbol{e}_{\rm p} = \boldsymbol{e}_{\rm p0}$. The new proper eccentricity vector $\boldsymbol{e}_{\rm p} = \boldsymbol{e}_{\rm p0} - \boldsymbol{e}_{\rm f}$ will mark the secular evolution of each planetesimal from then on. The modulus of the new $\boldsymbol{e}_{\rm p}$ ranges from $|e_{\rm f} - e_{\rm p0}|$ and $e_{\rm f} + e_{\rm p0}$ with all intermediate values being possible, if the belt is enough crowded. The $\boldsymbol{e}_{\rm p}$s will be used, together with $\boldsymbol{e}_{\rm f}$, to compute the subsequent secular evolution featured by circles centred on the tip of $\boldsymbol{e}_{\rm f}$ and with radius equal to $e_{\rm p}$. In the middle and lower panels of Fig. 2, we compare the analytic predictions of the secular theory with numerical integration of five different planetesimal orbits. They are all started with semimajor axis $a = 15$ au and all have the same value of initial eccentricity $e_{\rm p0} = 0.5 \cdot e_{\rm f}$. The pericentre longitude ϖ is set to 0°, 45°, 90°, 135° and 180°, respectively. In this way, we cover the most relevant secular behaviours typical of an initially warm belt perturbed by a planet. For small values of $e_{\rm p}$, a pseudo-libration around 0° is observed while for larger values circulation is restored. In all cases, there is a significant correlation between eccentricity and pericentre longitude.

In modelling warm belts, we will sample three different initial ratios between $e_{\rm p0}$ and $e_{\rm f}$, i.e. 0.25, 0.5 and 1. Linking $e_{\rm p0}$ to $e_{\rm f}$ is an arbitrary choice but it is adopted to give an idea of how higher initial values of $e_{\rm p0}$ influence both $P_{\rm i}$ and $U_{\rm c}$, and it appears more robust than selecting random values of $e_{\rm p0}$. It is less arbitrary, it can be easily replicated and, in addition, it includes a radial dependence that may be present in the initial belt. At present, we do not have the means to reconstruct the past history of a warm belt and of the dynamical mechanisms that may have stirred it (planet formation, protoplanets roaming around, a phase of planet–planet scattering, etc.) and, as a consequence, many different initial distributions of the planetesimal proper eccentricities are conceivable. We focus in this paper on those where the proper eccentricity does not exceed the forced one and decreases with radial distance. For warm belts, we will explore a scenario where the dynamical excitation involves also the inclination modelling, together with the case with $i = 3°$, one with $i = 15°$.

If the planetesimal belt is densely populated, a strong collisional damping may occur even after the planet reached its close-by orbit. This damping is due to the loss of orbital energy after each collision and, on average, it causes a reduction of the proper eccentricity $e_{\rm p}$. Any crowded belt might be drag to a condition similar to that illustrated in Fig. 3 even in the presence of a perturbing planet. The proper eccentricity is smaller than the forced one, and all planetesimals evolve in pseudo-librating orbits with a degree of alignment that depends on the ratio between proper and forced eccentricity. We will model also this dynamical configuration and compute values of $P_{\rm i}$ and $U_{\rm c}$ in this scenario.

We have to point out that our estimates of $P_{\rm i}$ and $U_{\rm c}$ cannot be applied to very young belts, since our model requires a full randomization of the pericentre of the planetesimals. This occurs on a time-scale of some tens of Myr when the perturber is a Jovian-type planet limiting the applicability of our computations to older discs. From equation (3), we can deduce that smaller sized planets need more time to randomize the pericentre since the secular period is inversely proportional to the planet mass $m_{\rm pl}$. For example, a Neptune-sized planet would lead to pericentre randomization on a time-scale approximately 20 times longer, i.e. about half of a Gyr. Our estimates of $P_{\rm i}$ and $U_{\rm c}$ will be valid only after that time.

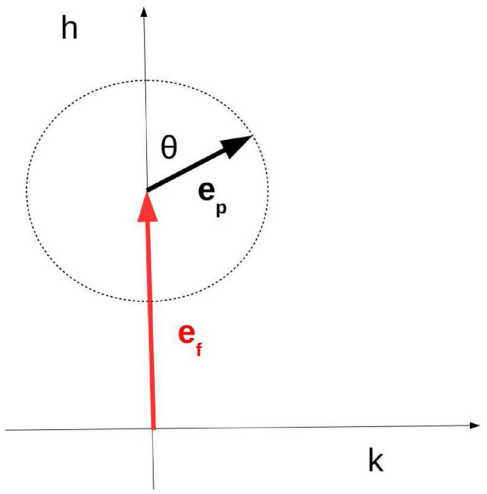

Figure 3. If the planetesimal belt is densely populated, a significant collisional damping may occur reducing the proper eccentricity even after the planet ignited its secular perturbations. In this case, the secular evolution will lead to pseudo-librations of the pericentre of all bodies and the secular evolution is described by the dashed circle.

3 THE METHOD

An essential prerequisite to model the collisional evolution of a population of minor bodies, like planetesimals, is a quantitative estimate of two parameters: the average impact velocity $U_{\rm c}$ and the intrinsic probability of collision $P_{\rm i}$. The impact velocity appears in all basic steps determining the outcome of a collision, and it discriminates between accumulation, cratering or shattering events. Together with semi-empirical scaling laws describing the strength of a body suffering a collision, $U_{\rm c}$ determines the mass of the largest remnant body and the size distribution of the escaping fragments. The intrinsic probability of collision $P_{\rm i}$ is related to the frequency of collisions between the bodies of the given population. It is a property related to the orbital distribution and defined independently from the number or size distribution of the bodies populating the belt. For example, for two given orbits, $P_{\rm i}$ is defined as the mean number per year of close encounters with minimum distance less than 1 km occurring between two points moving along the two orbits. If two bodies with radius $R_{\rm T}$ ('target') and $R_{\rm p}$ ('projectile') move along the above-mentioned orbits, the mean number of collisions per unit of time is $P_{\rm i}(R_{\rm T} + R_{\rm p})^2$. In wider terms, if the orbit of a target body with radius $R_{\rm T}$ moves within a swarm of $N_{\rm p}$ projectiles with radius $R_{\rm p}$, and $P_{{\rm i},\,k}$ is the intrinsic probability of collision between the target orbit and the orbit of the kth projectile, the mean number of collisions per unit of time suffered by the target is $\sum_k P_{{\rm i},\,k}(R_{\rm T} + R_{\rm p})^2$, or

$$\frac{{\rm d}n}{{\rm d}t} = \langle P_{\rm i}\rangle (R_{\rm T} + R_{\rm p})^2 N_{\rm p}, \tag{5}$$

where $\langle P_{\rm i}\rangle = (\sum_k P_{{\rm i},\,k})/N_{\rm p}$ is the *mean* intrinsic probability of collision (Farinella & Davis 1992; Davis et al. 2002). In this paper, we will treat only the cases of targets impacted by populations of projectiles, so hereinafter we use the symbol $P_{\rm i}$ always with the meaning of mean intrinsic probability of collision. It has been computed for

different populations of minor bodies in the Solar system and, for instance, its mean value for the asteroid belts is $P_i \sim 2.9 \times 10^{-18}$ km^{-2} yr^{-1} (Bottke et al. 2002). The important aspect of P_i is that it is not simply a particle-in-a-box model where the bodies move freely between collisions, but it accounts for the Keplerian dynamics of the bodies even when they are on perturbed orbits.

In the case of planetesimal belts perturbed by a planet in a close-by orbit, the classical Öpik/Wetherill approach for the computation of P_i and U_c cannot be used if the forced eccentricity is not significantly smaller than the proper eccentricity. The Öpik/Wetherill statistics, hereinafter termed 'canonical' statistics, is based on the following assumptions:

(1) the semimajor axes a, eccentricities e and inclinations I of the osculating orbits are fixed;
(2) the rate of variation of the node longitudes Ω and pericentre arguments ω of the osculating orbits are constant. In other words, the osculating orbits circulate uniformly;
(3) the motion of the planetesimals along their osculating orbits is fully described by the second Kepler's law.

The first attempt to overcome the assumptions of the canonical statistics has been done by Dell'Oro & Paolicchi (1997, 1998) and Dell'Oro et al. (1998). In particular, Dell'Oro & Paolicchi (1998) developed a mathematical formalism for the study of the statistics of collisions among asteroids provided that the following more general assumptions are fulfilled:

(1) the orbital parameters a, e and I of the osculating orbits are fixed;
(4) none of the osculating elements a, e and I is correlated with one of the angular elements Ω, ω or mean anomaly M.

Indeed, thanks to its numerical implementation, the method of Dell'Oro & Paolicchi (1998) can be used even if condition (1) is not fulfilled by simply substituting the ensemble of fixed values of a, e and I with a fictitious list of 'child' elements a, e and I whose distributions fit ad hoc parent distributions. So, in general, in all cases where condition (4) is fulfilled, the method proposed by Dell'Oro & Paolicchi (1998) can be employed. Unfortunately, the dynamical behaviour of a planetesimal belt perturbed by a planet strongly violates condition (4) because of the strong correlation between eccentricity and perihelion longitude, entailing a correlation among e, Ω and ω. To account for this correlation, we envisioned a different technique described here below.

Our new algorithm adopts a Monte Carlo approach consisting in a random exploration of the phase space of positions and velocities of the bodies in order to derive their rate of collision and impact velocity distribution. It can be summarized in four consecutive steps.

In the first step, a numerical model of the disc is prepared by generating a list of bodies with semimajor axis randomly and uniformly chosen in an interval $[a_{min}, a_{max}]$. Different radial distributions can be implemented, but in this paper we adopt this simple assumption that implies a decrease of the planetesimal superficial density as r^{-1}. The forced eccentricity for each body is computed from equation (2) (Mustill & Wyatt 2009) while the inclination I is randomly generated from a uniform distribution in the interval $[0, I_{max}]$. Finally, a value of proper eccentricity e_p is computed for all bodies that is derived from the initial assumed value of proper eccentricity e_{p0} of each planetesimal in the belt before it is perturbed. In all our models, the average number of bodies (orbits) used in the Monte Carlo statistics is of the order of 10 000. Our final goal is to compute the statistical parameters P_i and U_c for collisions occurring between all bodies belonging to our list, considered representative of the structure of the disc, and some selected target bodies (tracers) whose orbits have inclination $I_T = I_{max}/2$, semimajor axes a_T chosen at fixed steps between $[a_{min}, a_{max}]$ and values of e_p, e_f computed with the same rules for the disc bodies. In this way, P_i and U_c are functions of the semimajor axis of the target only and can be evaluated at different locations on the disc. In the case of a warm belt, since the tracers may have different values of e_p, 1000 tracers are used for each semimajor axis and the values of P_i and U_c are computed as average over all of them.

The second step consists of a random sampling of the mean anomaly M and of the secular angle θ, the angle between the vectors describing the proper and forced eccentricity, respectively (see Fig. 1). Both samplings are performed assuming a uniform distribution of the angles since we know from the secular theory that θ precesses at a regular pace, at least as a first approximation, while the mean anomaly M circulates with the constant frequency n. From the values of e_f, e_p and θ, we can derive the osculating eccentricity completing the set of orbital elements. From the long list of orbital elements sampled for each body of the disc and tracers, we can compute the list of positions and velocities ($\boldsymbol{r}_t$, $\boldsymbol{v}_t$, $\boldsymbol{r}_p$, $\boldsymbol{v}_p$) of projectiles and targets. This two-step sampling allows us to reproduce in the phase space, described by positions and velocities, the distribution of the orbital elements of projectiles and targets imposed by the secular perturbations of the planet. This distribution is characterized by different levels of correlation between e and $\tilde{\omega}$ that depend on the initial choice of e_{p0}. At this point, we have a model disc reflecting the secular dynamics in Cartesian coordinates.

The third step consists in computing, from the distribution of the positions and velocities of both projectiles and targets, the rate of close approaches and the distribution of impact velocities. For each target, the number $\nu(R)$ of close encounters within a given distance R per unit time is, by definition, the ratio

$$\nu(R) = \frac{N(R, T)}{T}, \tag{6}$$

where $N(R, T)$ is the number of close encounters occurred during an interval of time T and within a distance R. It is noteworthy that, in the context of the above equation, R is the distance between the centres of the two bodies during the approach and it is not the radius of either of the two bodies. Assuming a general dynamical stability of the system and choosing T long enough, the number $\nu(R)$ no longer depends either on the initial conditions of the system or on the value of T. We can rewrite this ratio as

$$\nu(R) = \frac{N(R, T)}{S(R, T)} \frac{S(R, T)}{T}, \tag{7}$$

where $S(R, T)$ is the sum of the durations of all close encounters occurred during the interval of time T and within the distance R. The ratio

$$\tau(R) = \frac{S(R, T)}{N(R, T)} \tag{8}$$

is the mean value of the durations of the close encounters within a distance R, while

$$p(R) = \frac{S(R, T)}{T} \tag{9}$$

is the probability to find a projectile within a distance R from the target at a randomly chosen instant of time. The mean close encounter duration $\tau(R)$ is related to the properties of the relative motion between projectile and target. Assuming that the relative trajectory of the bodies can be approximated as a rectilinear motion with constant velocity $v = |\boldsymbol{v}_t - \boldsymbol{v}_p|$, the average (expected) duration of a close encounter is $(4/3)(R/v)$, taking into account that the

projectile can pass anywhere inside the sphere of radius R around the target. This rectilinear motion approximation is valid only for values of the close approach distance R significantly smaller than the size of the orbits of the planetesimals. The probability $p(R)$ is directly derived from the $(\boldsymbol{r}_t, \boldsymbol{v}_t, \boldsymbol{r}_p, \boldsymbol{v}_p)$ list by computing the ratio between the number of samples for which $|\boldsymbol{r}_t - \boldsymbol{r}_p| < R$ and the total number of samples. In this way, the rate of the close encounters can be expressed in terms of the sampled quantities as

$$\nu(R) = \frac{3}{4}\frac{1}{\mathcal{N}R}\sum_k v_k, \tag{10}$$

where v_k is the relative velocity of the kth sample of target–projectile pairs. The sum includes only those cases for which $|\boldsymbol{r}_t - \boldsymbol{r}_p| < R$ while $\mathcal{N}$ is the total number of samples (Dell'Oro 2016).

The rate $\nu(R)$ is derived as a function of the close approach distance R. By definition of intrinsic probability of collision, $P_i = \nu(R)$ if $R = 1$ km. On the other hand, due to the numerical limitations of the Monte Carlo approach, it is not possible to evaluate the rate $\nu(R)$ directly for $R = 1$ km, since it requires an excessive computational effort. Nevertheless, for values of R small compared to the linear dimensions of the orbits, the rate ν is expected to be proportional to the geometric cross-section, that is $\nu(R) \propto R^2$ (the effect of the gravitational focusing is negligible due to the small sizes of the planetesimals). For all the cases investigated in this work, we have verified that $\nu(R)$ is really proportional to R^2 when R is small enough. For this reason, we extrapolate the function $\nu(R)$ down to $R = 1$ km by assuming that the R^2 trend is maintained. In short, within the interval of values of R for which $\nu(R)$ results to be proportional to R^2, the ratio $\nu(R)/R^2$ provides the value of P_i directly.

Together with P_i, we also compute the mean $\overline{v}(R)$ of the relative velocity for all close encounters with $|\boldsymbol{r}_t - \boldsymbol{r}_p| < R$. The parameter $\overline{v}(R)$ is correctly evaluated on the basis of the $(\boldsymbol{r}_t, \boldsymbol{v}_t, \boldsymbol{r}_p, \boldsymbol{v}_p)$ list as

$$\overline{v}(R) = \frac{\sum_k v_k^2}{\sum_k v_k}, \tag{11}$$

where again v_k is the relative velocity of the kth target–projectile pair and the sum includes only those cases for which $|\boldsymbol{r}_t - \boldsymbol{r}_p| < R$. From equation (10), it can be deduced that each of the target–projectile pairs contributes to the final evaluation of the frequency $\nu(R)$ with a term v_k/R. This comes from the fact that each orbital geometry has its own probability to occur, as outlined by Bottke et al. (1994). In other words, each value of the relative velocity v_k of the planetesimal ensemble has to be weighted by v_k itself in order to obtain the correct probability distribution of the relative velocities. The same holds true for any other parameter related to close encounters. But unlike $\nu(R)$, the value of $\overline{v}(R)$ is expected to tend asymptotically to a finite value for R smaller and smaller. This limit is the mean value U_c of the impact velocity. In general, for the cases under investigation in this work, we have verified that the function $\overline{v}(R)$ decreases for lower R and it becomes constant from a certain value onwards, providing our estimation of U_c.

The procedure described above leads to an accurate estimate of both P_i and U_c (Dell'Oro 2016). The algorithm has been extensively validated on different sets of test cases and, in particular, it provides values of P_i and U_c for main belt asteroids and Kuiper belt objects that are in agreement with those previously reported in the literature.

The direct source of uncertainty in the computation of P_i and U_c is due to the casual fluctuations in the random sampling of the phase space, depending on the total number of samples (and so the total duration of the computation). Another, but indirect, error is introduced by the fluctuations in the construction of the ring model. The list of planetesimal orbits is generated randomly and not all the particles in the ring intersect the orbit of the target, but only a fraction of them within a more or less wide range of semimajor axes. This means that, depending on the details of the random generation of the orbits, the number of bodies intersecting the orbit of the target can change a little, impacting on the evaluation of P_i and U_c. The total number of random samples has been tuned in order to constrain the uncertainties within few per cent of P_i and U_c.

4 THE 'STANDARD' CASE

As a first test, we apply our algorithm to compute the intrinsic probability of collision and average impact velocity to a 'standard' case similar to that explored by Mustill & Wyatt (2009). In this model, a planetesimal belt extends from 10 to 20 au, and it is perturbed by a Jupiter-sized planet with mass $m_p = 0.001$ $M_\odot$ on an orbit with semimajor axis $a_{pl} = 5$ au while the eccentricity can be either $e_{pl} = 0.1$ or 0.6. We consider two distinct configurations: a cold belt that, before the arrival of the planet in a perturbing orbit, had a very low proper eccentricity ($e_{p0} \sim 0$). In this case, when the planet turns on its secular perturbations, the value of e_p becomes approximately equal to e_f (see Fig. 1). We also explore the evolution of warm belts that, prior to the planet arrival, had already a high value of proper eccentricity e_{p0}, possibly excited by other mechanisms like an extended period of planet–planet scattering or the formation of large embryos. In this scenario, we assume that e_{p0} is a significant fraction of e_f and we test three cases, one with $e_{p0} = 0.25 \cdot e_f$, one with $e_{p0} = 0.5 \cdot e_f$ and one, the most excited, with $e_{p0} = e_f$. This is just an arbitrary choice to show the effects of an initial value of $e_{p0} > 0$, and it is not dictated by any particular scenario. It appears a better choice than a random selection of e_{p0} values. As soon as the planet begins to perturb the warm belt, the eccentricity values will be encompassed between $e_f - e_p$ and $e_f + e_p$, where e_p is derived from the initial value of e_{p0} as described in Section 2 (see Fig. 2).

4.1 Initially cold belt

In an initial cold belt, the correlation between e and ϖ that the planet establishes when approaching the belt is the strongest due to the assumption that $e_{p0} = 0$. The secular dynamics is well described by the plots of Fig. 1. Both P_i and U_c are shown in Fig. 4 as a function of the semimajor axis of the tracers that well approximate the average radial distance from the star of each body. In this figure, we illustrate the case with $e_{pl} = 0.1$, a configuration in which the planetesimal belt is less perturbed (compared to $e_{pl} = 0.6$). The green filled squares are the impact velocity values computed assuming that there is no secular correlation between the eccentricity and perihelion longitude (hereinafter the 'canonical' case) while the red open squares show the probability and velocity values when the secular correlation is taken into account. The dotted line in the lower panel of Fig. 4 gives the average relative velocity computed as $U_c = 1.4 e_f v_{kep}$, where v_{kep} is the local Keplerian velocity (Mustill & Wyatt 2009). This relation leads to a simple $r^{-3/2}$ scaling of the velocity with the radial distance r. The correlation between eccentricity and perihelion longitude reduces both P_i and, in particular, the relative impact velocity U_c with respect to the case without secular correlation. This is due to two effects that are manifested in Fig. 1: there is a consistent fraction of orbits with very low eccentricity while the high eccentric orbits have their pericentres almost aligned around 0° leading to low-velocity impacts.

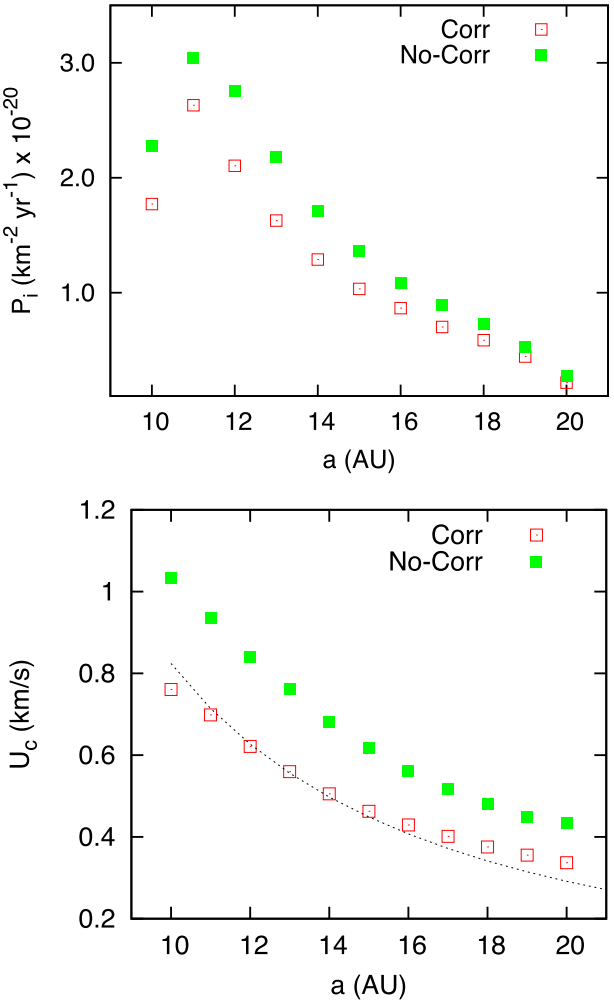

Figure 4. Intrinsic probability of collision P_i (top panel) and impact velocity U_c (bottom panel) for a planetesimal belt perturbed by a Jupiter-sized planet with $a_p = 5$ and $e_p = 0.1$. The belt is assumed to have been initially cold so that $e_p = e_f$. The green filled squares mark the predictions of the canonical model where no secular correlation is assumed between e and ϖ while the red open squares are the values computed with the model that include the secular correlation. The dashed line in the bottom panel outlines the values derived from the analytic formula $U_c = 1.4 e_f v_{kep}$ (Mustill & Wyatt 2009).

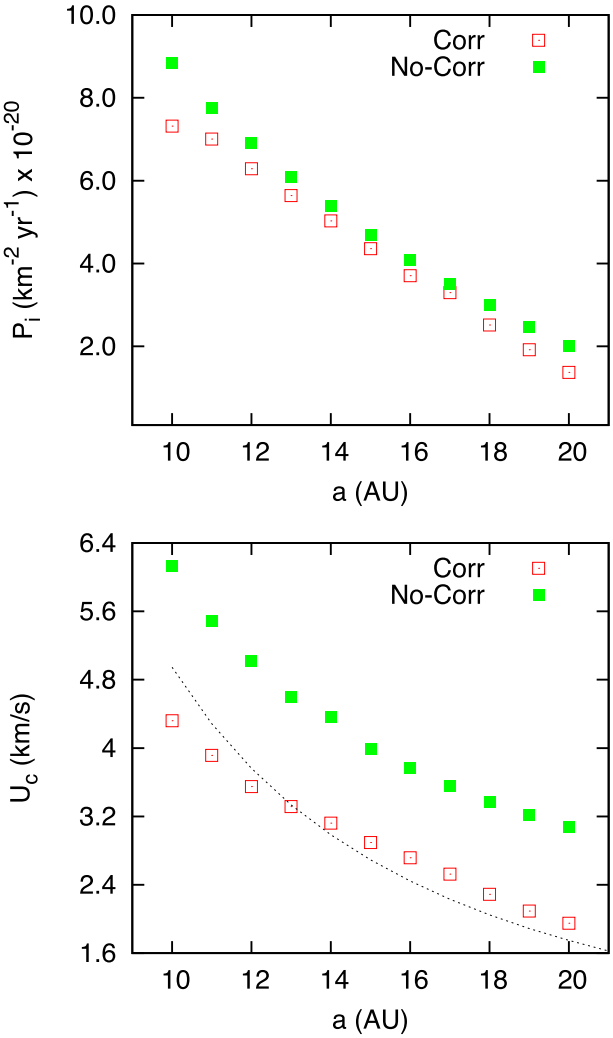

Figure 5. Same as Fig. 4 but for $e_p = 0.6$.

The analytic prediction of Mustill & Wyatt (2009) for U_c appears to slightly overestimate the impact speed at 10 au by about 10 per cent and underestimate it at 20 au by approximately the same amount. The $r^{-3/2}$ scaling does not appear to fully account for the dynamical evolution of the belt possibly because it does not properly account for the spatial distribution of the encounters' radial locations related to the secular dynamics. For P_i, it is difficult to derive a proper scaling with the radial distance since two different effects come into play in determining P_i as a function of r. On one side, there is a pure dynamical dependence of the probability of collision of a planetesimal pair on r related to their orbital elements. A typical equation giving such a probability can be found in Wetherill (1967, equation 20). However, we are computing the P_i not of a single pair, but for an entire population of planetesimals and their radial distribution comes strongly into play. This radial distribution does not only depend on the planetesimal superficial density distribution but it is significantly influenced by the distribution of all orbital elements of the population. As a consequence, it cannot be predicted a priori with an easy power-law distribution, in particular for highly eccentric belts.

Close to the inner edge of the belt, the value of P_i decreases due to the inner truncation of the belt and to a reduction in the number of crossing orbits. This effect will disappear for higher eccentricities since the perihelion–aphelion radial distance is larger for the planetesimals and the orbital crossing is more extended.

In Fig. 5, we show both P_i and U_c when the eccentricity of the planet is increased to 0.6, a significantly more perturbed configuration for the planetesimal belt. The value of P_i is increased by about a factor of 4 leading to a very active belt in terms of collisions while the impact velocity U_c is five times higher compared to the case with $e_{pl} = 0.1$ and comparable to the value of the present asteroid belt. The vast majority of collisions are expected to be highly energetic, and both fragmentation and cratering are possibly dominant leading to a high rate of dust production. These results show that a higher eccentricity of the planet not only leads to higher impact speeds but it substantially increases the impact rate (larger P_i) that is possibly more important in producing brighter debris discs.

Our numerical algorithm allows us to compute the contribution to the average P_i and U_c coming from a restricted arc of the trajectory of the target, or, more precisely, from a given range of values of the

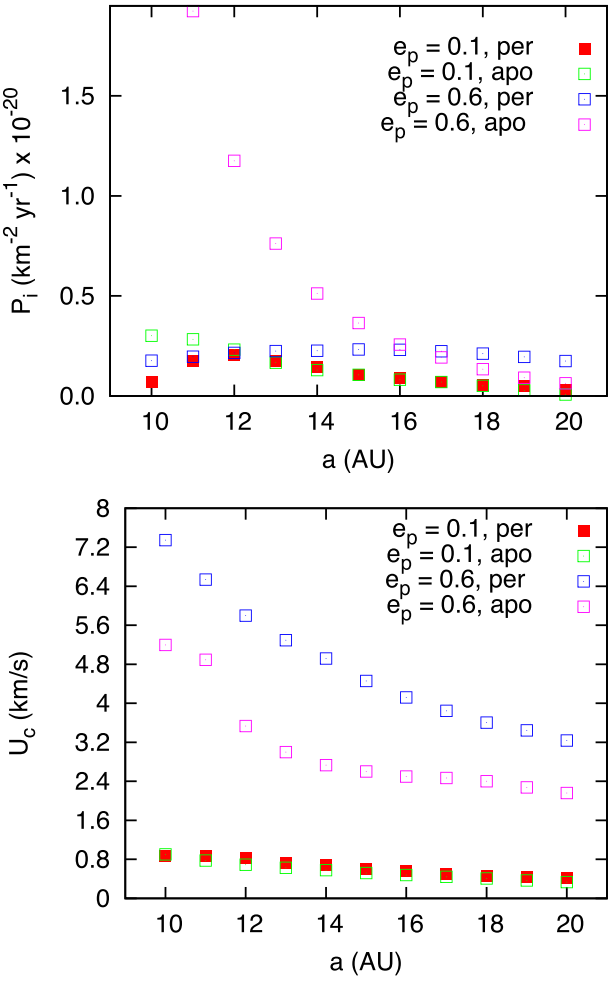

Figure 6. Intrinsic probability of collision P_i (top panel) and impact velocity U_c (bottom panel) computed around the pericentre ($-15^\circ < f < 15^\circ$) and apocentre ($165^\circ < f < 195^\circ$) of all targets. The eccentricity of the planet is set to $e_p = 0.1$ and 0.6.

true anomaly f. Thanks to this feature, we can evaluate the frequency of collision and impact velocity around the pericentre and apocentre, respectively. We have selected a range of $\pm 15^\circ$ around both $f = 0^\circ$ and $f = 180^\circ$ for each target in order to underline different values of P_i and U_c in these restricted ranges. The results are shown in Fig. 6 for the models in which the eccentricity of the planet is set to $e_p = 0.1$ and 0.6, respectively.

When $e_p = 0.1$, the difference between P_i and U_c at the pericentre and apocentre is small. However, when $e_p = 0.6$, a significantly higher value of P_i is observed when the target is at the apocentre and hence in the inner regions of the belt. Beyond 17 au, the trend reverses and P_i becomes larger at the pericentre. This behaviour is due to the high forced (and then proper) eccentricity induced by the secular perturbations of the planet. When the target is close to the inner border of the belt, its pericentre is located where the density of potential projectiles is significantly lower due to the overall eccentricity distribution ranging from 0 and $2\,e_f$. On the other hand, when the target orbits around the apocentre, it is well within the belt where the density of the projectiles is the highest and P_i is large. Moving towards the outer border of the belt, it is now the apocentre of the targets that is located in low-density regions while the pericentre is well within the belt, and this leads to higher values of P_i. Superimposed to this effect there is also the decreasing trend of P_i for larger values of a due to a reduction of both the forced eccentricity and radial density of the planetesimal population. The values of P_i shown in Fig. 6 are only a fraction of the total impact probability illustrated in Fig. 5 since we are considering only a portion of the total range of the true anomaly f and, as a consequence, they are substantially smaller than the values in Fig. 5.

Significantly different values of U_c are also found at the pericentre and apocentre when $e_p = 0.6$. At the apocentre, the values of the impact speed are comparable with the average values shown in Fig. 5 but at pericentre U_c is much higher since the target has a higher orbital velocity compared to the potential projectiles. Due to the correlation between e and ϖ, a significant number of impacts when the target is at the pericentre occur with circular orbits having radius approximately equal to $a(1 - e)$. By comparison, at the apocentre the target will frequently encounter projectiles on circular orbits with radius $a(1 + e)$. As a consequence, at the pericentre the impact velocity U_c is higher.

4.2 Initially warm belt

In a scenario where the planet is injected in an orbit perturbing an already heated planetesimal belt, the values of P_i and U_c are different with respect to those of a cold belt because of the changes in the secular dynamics (Fig. 2). Here we consider three test cases where the proper eccentricity e_{p0}, before the onset of the planet perturbations, is 0.25, 0.5 and 1.0 that of the forced eccentricity (the value that will be established once the planet approaches the belt). Different values of e_{p0} can be encountered in real systems, and our choice to link e_p to e_f is arbitrary, but it is impossible to explore all possible initial distributions of e_{p0}, so we consider only three reference cases, where e_{p0} is linearly related to e_f, which give clues on how to deal with any general scenario.

In Fig. 7, we compare P_i and U_c when $e_{pl} = 0.1$ for all the different initial configurations corresponding to distinct dynamical states of the belt prior to the onset of the planet perturbations, i.e. cold and warm belts. This comparison highlights the effects on P_i and U_c of different degrees of correlation between e and ϖ related to the distinct initial values of e_{p0}. Both the intrinsic probability of collision and impact velocity increase for higher values of e_{p0} (initially warm belts) until, for $e_{p0} = e_f$, values comparable to those of the uncorrelated case (the canonical one) are obtained. This increase is due to the complex interplay of dynamical effects that can be deduced from Fig. 2. First of all, in warm belts higher eccentricity values are achieved since e_p ranges from $e_f - e_{p0}$ to $e_f + e_{p0}$ with respect to the cold scenario where $e_p = e_f$. In addition, when the pericentre ϖ is around 180°, the planetesimal eccentricities are not all small as illustrated in Fig. 1 but they may reach significant values (Fig. 2). Finally, pseudo-librators, whose fraction depends on the initial value of e_{p0}, impact with non-librators leading to geometrical configurations where the trajectories at the crossing are more bent and favour larger collisional velocities. All these mechanisms contribute to increase both P_i and U_c up to values similar to those of the canonical case also when $e_{pl} = 0.6$, as illustrated in Fig. 8.

Our numerical models show that initial warm belts have a more intense collisional activity due to higher values of both P_i and U_c. This leads to a greater production of dust and a brighter debris disc associated with the belt but also to a faster erosion rate with a shorter lifetime.

The value of impact velocity U_c shown in the previous plots is indeed an average over a large number of computed impact speeds. The velocity distribution in the standard case with $e_{pl} = 0.6$ for the

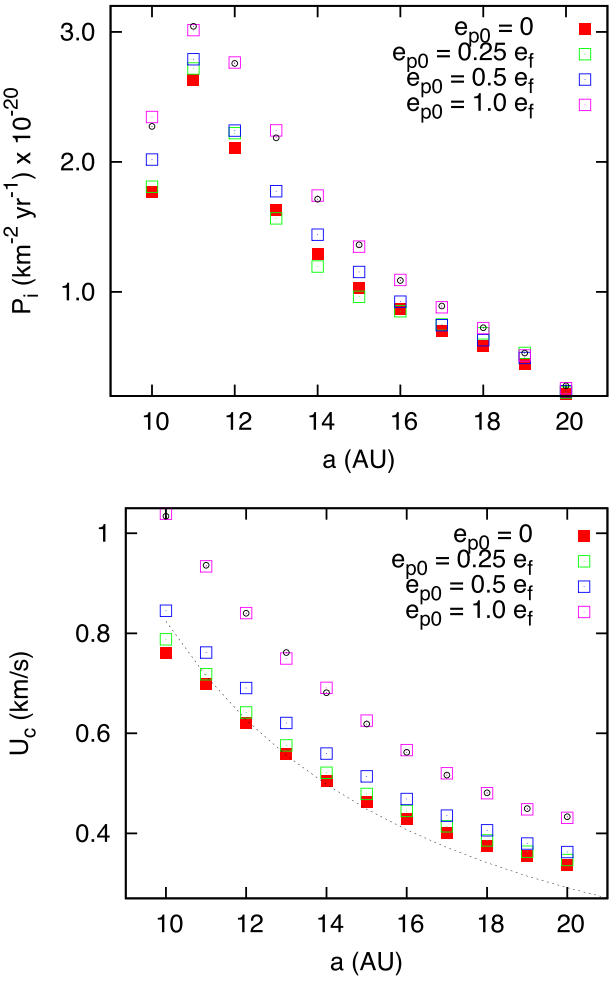

Figure 7. P_i (upper panel) and U_c (lower panel) for initially warm and cold belts. For the warm belts, we assume three different values of e_{p0}, i.e. 0.25 (green open squares), 0.5 (blue open squares) and 1 times e_f (magenta open squares). The red filled squares mark the values of P_i and U_c for a cold belt while the black open circles show the case with $e_p = e_f$ *without* secular perturbations. The eccentricity of the perturbing planet is set to $e_{pl} = 0.1$.

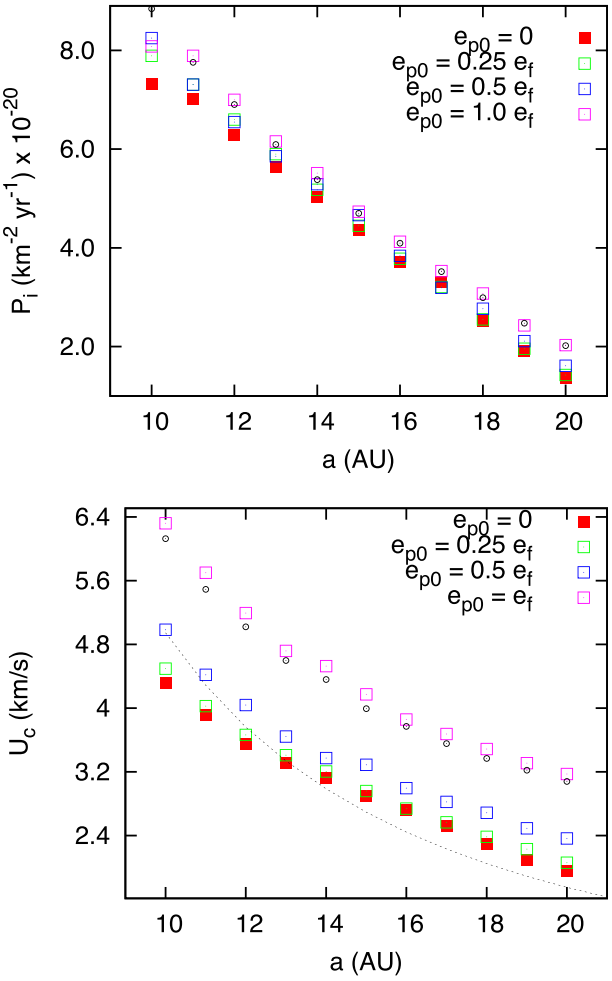

Figure 8. Same as Fig. 7 but for $e_{pl} = 0.6$.

target with $a_T = 15$ au is displayed in Fig. 9. The black dashed line shows the impact velocity distribution in the absence of e–ϖ correlation (a warm belt not perturbed by a planet) while the red continuous line illustrates the distribution when such correlation is included in the computation of U_c for an initially cold belt. The high-velocity tail of the distribution is cut off and this explains the reduction in the average impact speed observed in Fig. 5. In the warm case with $e_{p0} = 0.5e_f$, the cut-off at high impact speeds is reduced compared to the case with $e_{p0} = 0$ due to the contribution of pseudo-librators impacting circulators. However, the peak is located at lower impact speeds and the average value of U_c is still lower compared to the case without e–ϖ correlation.

4.3 Initially warm and inclined belt: $i = 15°$

In the presence of a strong dynamical excitation, due to possible different mechanisms like self-stirring, the presence of large planetary embryos, resonance sweeping, etc., even the osculating inclinations may be significantly pumped up. We explore in this section the effects of increasing the average value of inclination on the values of P_i and U_c. Intuitively, one would expect an increase in the relative

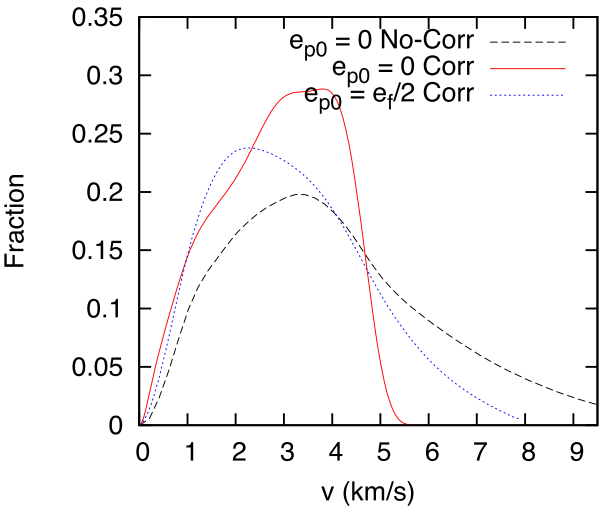

Figure 9. Normalized impact velocity distribution for $e_p = e_f$ without the secular correlation between e and ϖ (black dashed line) and for the case in which such correlation is included in the computations (red continuous line). The blue dotted line illustrates the velocity distribution for a warm belt with $e_{p0} = 0.5 \cdot e_f$.

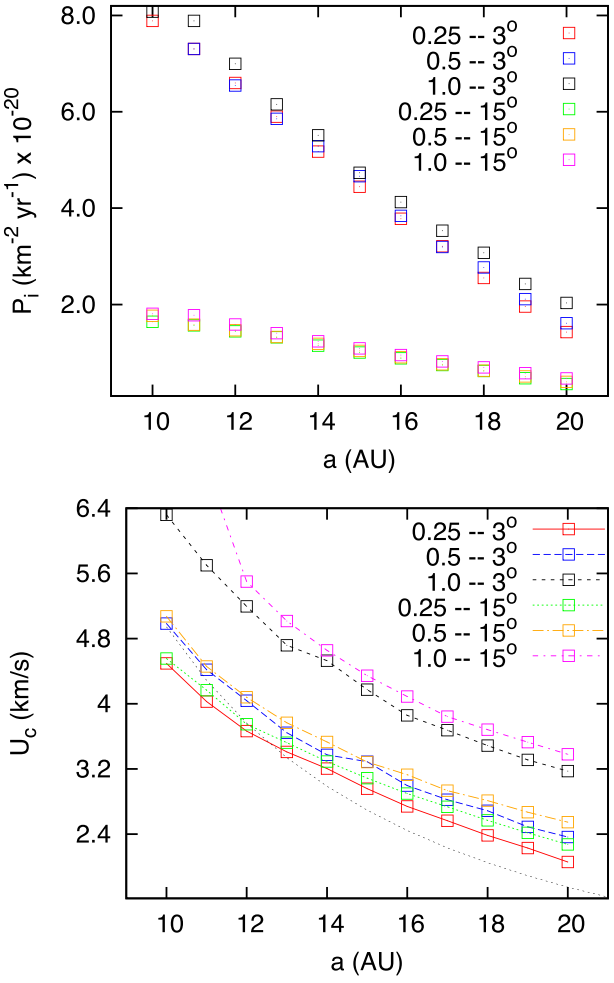

Figure 10. Intrinsic probability of collision P_i and impact velocity U_c for a small body belt with $e_{p0} = 0.25$, 0.5 and 1.0 e_f and $i = 15°$, compared to the values computed for $i = 3°$. The perturbing planet has an eccentricity $e_{pl} = 0.6$. While P_i is significantly reduced, the impact velocity U_c is approximately increased by 40 per cent.

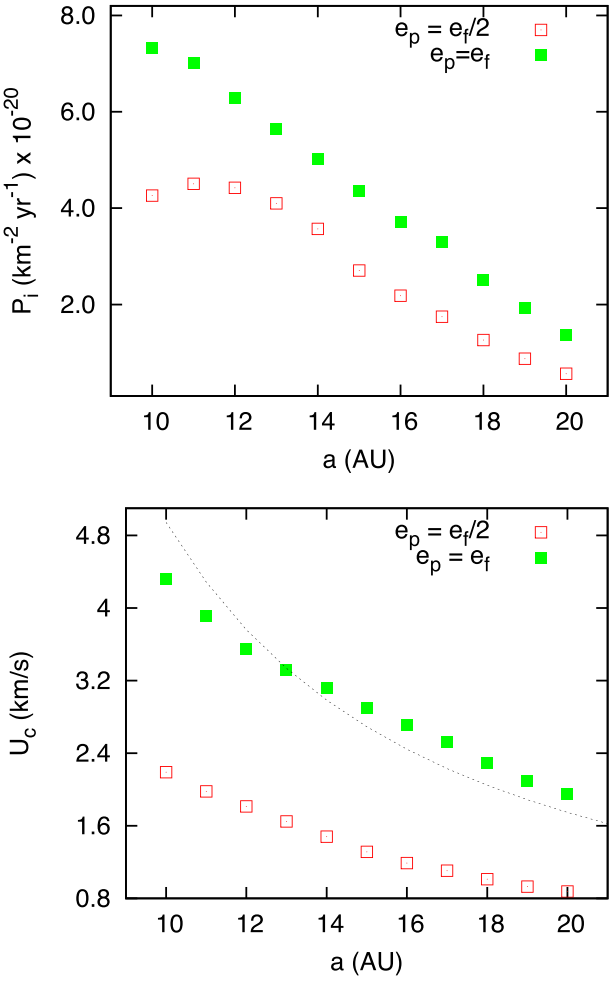

Figure 11. Intrinsic probability of collision P_i and impact velocity U_c for a small body belt collisionally damped after the onset of the planet perturbations. The eccentricity of the planet is set to 0.6 and the proper eccentricity is assumed to have been damped to a value $e_p = 0.5 \cdot e_f$. Both P_i and U_c are compared to the values computed for a non-damped cold belt (green filled squares). There is a significant decrease of both P_i and U_c due to the pseudo-libration of all planetesimals.

impact velocity due to the presence of an additional out-of-plane component in the difference between the velocity vectors of two planetesimals. At the same time, due to an expansion of the available space for orbital motion, a significant decrease of the impact probability is expected. Both these predictions are confirmed by the outcome of our algorithm, and in Fig. 10 we show the computed values of P_i and U_c for initially warm belts with $e_{p0} = 0.25, 0.5, 1 \cdot e_f$ and an average inclination of 15° (the perturbing planet has $e_{pl} = 0.6$). The exploration of larger values of inclination would require a more detailed secular approach where the inclination is coupled to the node longitude and this will be done in a forthcoming paper.

In the case of inclined belts, the value of P_i in the inner regions of the belt is reduced by about a factor of 4 compared to the case with $i = 3°$ (see Fig. 10). On the other hand, the impact velocity U_c is higher for more inclined planetesimals due to the out-of-plane component in the relative velocity, reaching a maximum value of 8 km s^{-1} at 10 au from the star when $e_{p0} = 1 \cdot e_f$ (magenta open squares in the bottom panel of Fig. 10). However, a higher inclination appears to be not as important as a higher value of e_{p0} in leading to higher impact speed. In general, according to our modelling, an inclined belt is expected to be less collisionally active due to the strong decrease in P_i, in spite of an increase of U_c. This will be confirmed by the collisional evolution models of the next section.

4.4 Collisionally damped belt

We consider here the case of a densely populated belt whose proper eccentricity distribution, after the approach of the planet, has been collisionally damped. In this scenario, most of the orbital excitation is dissipated and the proper eccentricity is reduced to values smaller than the forced one. This would lead to the dynamical state illustrated in Fig. 3 where all the planetesimals are in pseudo-libration. We compute the intrinsic probability of collision and impact velocity when the damped configuration is reached. To model this kind of belt, we select a value of proper eccentricity, after the damping, which is half the value of the forced one. Even in this case, the choice is made to give an idea of the influence of this secular configuration on the collisional evolution of the belt, i.e. on the values of P_i and U_c, and it is not related to any particular scenario.

For a damped belt, both P_i and U_c are reduced (see Fig. 11) and this has to be ascribed to the pseudo-libration of all planetesimals.

ϖ oscillates within a limited range around 0° leading to a significant level of pericentre alignment of all orbits. This dynamical configuration leads to collisions where the trajectories of the approaching planetesimals are almost parallel at the orbital crossing. As a consequence, there is a consistent reduction of the impact velocity and impact rate. A damped belt is then expected to be less collisionally active and it will give rise to debris discs that are less bright.

5 COLLISIONAL EVOLUTION

To explore the implications of different values of P_i and U_c on the evolution of a planetesimal belt, we have run a simple one-dimensional collisional evolution code (Campo Bagatin et al. 1994; Marzari, Davis & Vanzani 1995; Bottke et al. 2005). We start from an initial planetesimal population extending from 10 to 500 km in diameter and distributed in a series of discrete logarithmic diameter bins following a slope equal to −3.5. The population is centred at 15 au and it is 10 au wide. The code computes the collisional interactions of each size bin with every other one during a given time-step. At the end of the time-step, all the outcomes of the interactions are summed up to find the net change in the population as a function of size. The updated population is then used in the next time-step until the whole time-span, which we assume to be 4 Gyr, is covered. These calculations are performed under the assumption that the orbital element distribution of the planetesimals is not significantly altered by the collisions so that both P_i and U_c remain constant during the entire evolution of the belt. Two different scaling laws for the computation of the fragment size distribution after a catastrophic impact are tested: a simple energy scaling like that proposed in Davis & Farinella (1997) to study the collisional evolution of Kuiper belt objects and the more recent one given in Stewart & Leinhardt (2009) for weak aggregates (their equation 2). The results are not significantly different so we report only those obtained with the scaling law of Stewart & Leinhardt (2009).

We have run four different models: two for cold belts with $e_{pl} = 0.1$ and 0.6, one for an initially warm belt where $e_{pl} = 0.6$ and $e_{p0} = 0.5 \cdot e_f$, and the last case for $e_{pl} = 0.6$, $e_{p0} = 0.5 \cdot e_f$ and $i = 15°$. The evolved planetesimal populations in the four different cases are shown in Fig. 12. When $e_{pl} = 0.6$, the erosion of the belt leads to a significant reduction in the number of planetesimals even at large sizes. Compared to the case with $e_{pl} = 0.1$, the simulation with $e_{pl} = 0.6$ shows an erosion rate about 10 times faster over 4 Gyr. A significant larger amount of dust is then expected to be produced when the eccentricity of the planet is higher, at least in the initial phases of evolution of the belt, as it could have been argued by the larger values of both P_i and U_c. However, old belts may have been significantly depleted by the initial fast collisional erosion and show at present a dust production rate comparable to or even lower than that of young and less depleted belts around low-eccentricity planets.

The collisional evolution of an initial warm belt with $e_{p0} = 0.5 \cdot e_f$ and $e_{pl} = 0.6$ is only slightly faster compared to an initial cold belt ($e_{p0} = 0$) and a similar dust production rate is expected. This shows that, in spite of an increase of the impact velocity U_c in the warm case, the two dynamical configurations lead to a similar collisional evolution because P_i is almost equal. This is confirmed also by the inclined case where a lower value of P_i leads to a less eroded belt in spite of a higher collisional velocity (see Fig. 10). This suggests that the intrinsic probability of collision is decisive in determining the erosion of a small body belt notwithstanding different values of impact velocity.

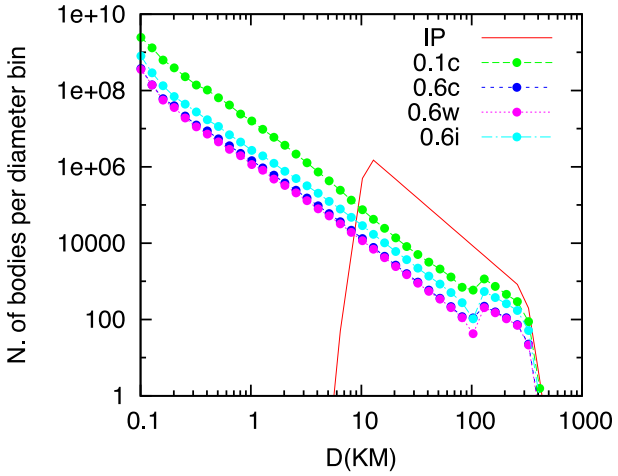

Figure 12. Collisional evolution over 4 Gyr of a putative planetesimal belt, centred at 15 and 5 au wide, for two different values of the planet eccentricity e_{pl}, i.e. 0.1 and 0.6, and for a warm and inclined population. The values of P_i and U_c used in the collisional evolution code are taken from the previous computations. The initial size distribution (red line), divided into a series of discrete bins, is truncated at 10 and 500 km in diameters. The erosion of the belt is faster in the case labelled *0.6w* (magenta circles) where $e_{pl} = 0.6$ and $e_{p0} = 0.5 \cdot e_f$, i.e. a warm belt. The initial cold belt with the same planet eccentricity (*0.6c*; blue filled circles) differs only slightly from the *0.6w* case. When the inclination of the warm belt is increased to 15°, the collisional evolution is reduced, as expected by the strong decrease of P_i (see Fig. 10). The case with $e_{pl} = 0.1$, labelled *0.1c*, illustrates the evolution of a cold belt perturbed by a low-inclination planet and it is the less collisionally active case.

The previous modelling must be considered only as indicative since additional information is needed in particular about the structural strength and porosity of the planetesimals since these physical aspects are heavily involved in the computation of the outcome of mutual collisions. In addition, this code is limited in the size range that it can cover and it does not possess spatial resolution. It cannot be compared with codes like DYCOSS and LIDT-DD (Thébault 2012; Kral, Thébault & Charnoz 2013) describing the evolution of a debris disc both in time and space, including effects like the Poynting–Robertson drag and creating a coupling between dynamics and collisions. The only advantage of our simplified code is that it can predict on the long term (time-scale of the order of Gyr) how the dust production rate will decline and establish a potential correlation between the age of the star and the luminosity of the belt. It can also be used in a reverse approach allowing us to determine the size distribution of the primordial belt from the present belt around an aged star, as it is usually done for the asteroid belt in the Solar system.

6 THE BELT IN HD 38529: COMPARISON WITH ϵ ERIDANI

HD 38529 is a complex system where two massive planets have been found to orbit the central body, a 3.5 Gyr old G8-type star. Their masses are 0.8 and 12.2 M_J and their orbital elements are $a_1 = 0.13$ au, $a_2 = 3.74$ au, $e_1 = 0.25$ and $e_2 = 0.35$, respectively (Butler et al. 2006). Moro-Martín et al. (2007b) found from *Spitzer* data an infrared excess that interpreted as due to the presence of a debris disc. From dynamical constraints, they located the dust-producing long-lived planetesimals in three regions. A small inner ring orbiting between the two planets from 0.4 to 0.8 au, a wider

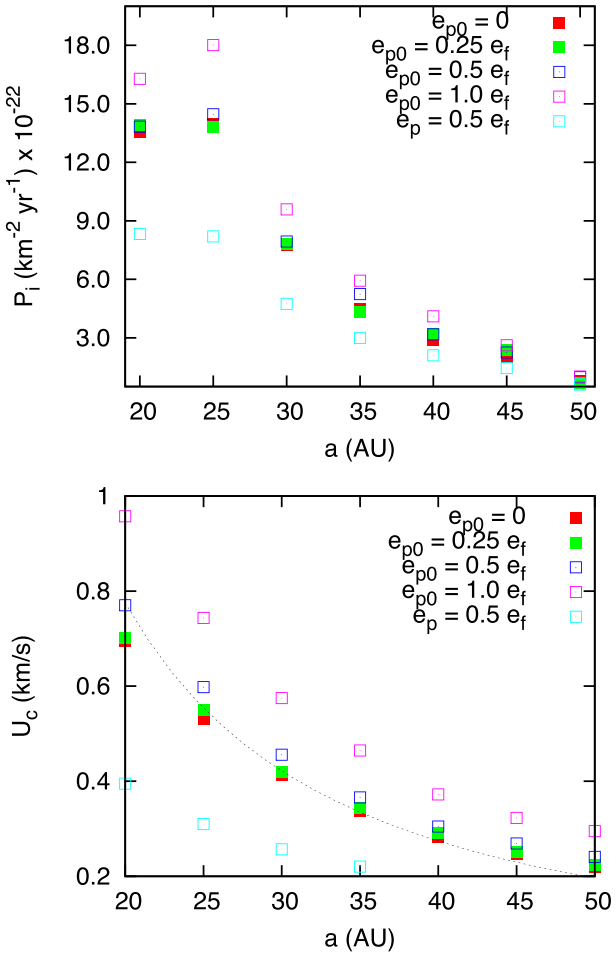

Figure 13. P_i (upper panel) and U_c (lower panel) for the belt observed in the HD 38529 system. We consider three different models: an initial cold belt with $e_p = e_f$ ($e_{p0} = 0$), an initial warm belt with different values of e_{p0} and a collisionally damped belt with $e_p = 0.5 \cdot e_f$.

outer belt extending from 20 to 50 au and an even outer one beyond 60 au. The two outer belts are separated from a strong secular resonance located at about 55 au. We focus our study on the belt extending from 20 to 50 au where Moro-Martín et al. (2007b) constrain the location of the dust-producing planetesimals. They in fact find that the debris disc is collision dominated implying that the planetesimals approximately share the same orbits as the emitting dust. We compute for this system the intrinsic probability of collision and impact velocity at different radial distances within 20 and 50 au. In Fig. 13, we show P_i and U_c for this belt. We consider only the outer more massive planet as perturber and we neglect the influence of the smaller inner one. Compared to the Kuiper belt in the Solar system, the intrinsic probability of collision appears to be larger in particular in the inner regions of the belt. According to Dell'Oro et al. (2001), P_i in the Kuiper belt ranges from 3.14 to 4.44×10^{-22} yr^{-1} km^{-2} while from Fig. 13 for 38529 P_i is at least three times larger in between 20 and 30 au. On the other hand, the impact velocity in the HD 38529 debris disc appears to be smaller than that in the Kuiper belt whose value is about 1.23–1.44 km s^{-1}. In short, in HD 38529 collisions are expected to be more frequent but less energetic.

By using the values of P_i and U_c at the centre of the belt (35 au; see Fig. 13), we run the collisional evolution code. In Fig. 14, the evolution with time of the size distribution of an initial planetesimal

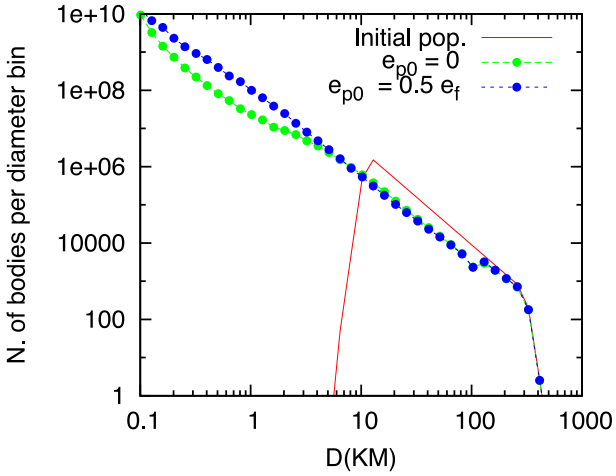

Figure 14. Collisional evolution of a planetesimal belt in the HD 38529 system. The erosion rate is much slower compared to that of the standard case shown in Fig. 12 due to the lower values of both P_i and U_c. The warm belt is slightly collisionally more active since a larger number of bodies are disrupted in between 10 and 40 km in diameter. These break-ups produce smaller fragments that refill the population at small sizes.

belt equal to that used for Fig. 12 is shown. Compared to Fig. 12, the shattering events are significantly reduced, and only a limited number of bodies smaller than 100 km in diameter are catastrophically disrupted. This must be ascribed to the lower value of P_i that is about 30 times smaller for the HD 38529 belt compared to the P_i of our standard case. The dust production rate is then expected to be significantly lower. The difference observed between the cold and warm cases at small sizes is due to the slightly larger number of big bodies disrupted in the warm belt, a phenomenon that can barely be seen in Fig. 12 in between 10 and 40 km. The fragments produced in these break-ups refill the size distribution at smaller diameters explaining the larger number of small bodies in the warm belt.

Together with HD 38529, also ϵ Eridani has a debris disc identified by dust emission (Greaves et al. 1998; MacGregor et al. 2015). The belt is supposed to extend from approximately 53 to 80 au from the central star, and it is perturbed by a giant planet with a mass approximately 1.66 times the mass of Jupiter and on an orbit with semimajor axis equal to 3.39 au and eccentricity of 0.7 (Benedict et al. 2006). This belt has approximately the same radial extension of that around HD 38529 (about 30 au) but it is located farther out from the star. The mass in the dust estimated in the ϵ Eridani debris disc is about 2×10^{-5} M$_\odot$, according to Li, Lunine & Bendo (2003). This value is significantly higher compared to that inferred for HD 38529 by Moro-Martín et al. (2007b) of 1–5 $\times$ 10^{-10} even if this was obtained for particles of 10 μm in size. A higher dust mass for ϵ Eridani can only partially be explained by the younger age of the system (about 800 Myr for ϵ Eridani versus 3.28 Gyr for HD 38529). We have computed the intrinsic probability of collision and impact velocity for the putative planetesimal belt precursor of the debris disc in ϵ Eridani. At the centre of the belt around 67 au, we find $P_i \sim 2 \times 10^{-23}$ km^{-2} yr^{-1} and an average impact velocity of about $U_c \sim 0.1$km s^{-1} while for HD 38529 in the centre of the belt at 35 au (see Fig. 13) we have $P_i \sim 4.5 \times 10^{-22}$ km^{-2} yr^{-1} and $U_c \sim 0.35$ km s^{-1} (assuming in both cases an initial cold belt). The collisional activity is then expected to be at least 20 times faster in HD 38529 with respect to ϵ Eridani. However, as shown in Fig. 14, the collisional evolution in HD 38529 cannot have led to a significant erosion of the belt even after 3.28 Gyr. Why is then the dust in

the debris disc around ϵ Eridani more dense than that around HD 38529? The only possible explanation is that the planetesimal belt in ϵ Eridani is significantly more populated with respect to that of HD 38529. The star of ϵ Eridani is less massive compared to that of HD 38529 (0.83 versus 1.39 $M_{\odot}$) so it is difficult to imagine that the protoplanetary disc around ϵ Eridani was much more dense than that around HD 38529. One possibility is that the dynamical history of HD 38529 has been more turbulent with extended periods of planet–planet scattering. This behaviour might have depleted the belt, as suggested by Bonsor et al. (2013) and Marzari (2014), leaving a lighter belt that subsequently evolved under mutual collisions. This evolution might explain the present difference between the two systems.

7 DISCUSSION AND CONCLUSIONS

The dust production rate in a debris disc, and then its brightness, strongly depends on the collisional evolution of the parent planetesimal belt. Since planetesimals are remnants of the planet formation process, it is then reasonable to expect that one or more planets formed in the system, notwithstanding any significant correlation between stars with dust emission and the presence of known planets is still under scrutiny. The collisional evolution of planetesimals and the dust production rate can be determined once both the physical structure of the bodies (in particular strength and porosity) and two fundamental dynamical parameters, the intrinsic probability of collision $P_{\rm i}$ and the mutual impact velocity $U_{\rm c}$, are known. While the physical structure of planetesimals depends on the dust accumulation process in the early phases of the circumstellar disc evolution, the values of the two parameters $P_{\rm i}$ and $U_{\rm c}$ are uniquely determined by the orbital architecture of the system. This in turn depends on planetesimal accumulation and planet formation but it is possibly influenced also by other evolutionary processes like planet migration by tidal interaction with the gaseous disc and phases of planet–planet scattering. This last mechanism is expected to have occurred in a significant fraction of systems due to the large number of exoplanets found in highly eccentric orbits. Planet–planet scattering not only excites eccentricity but it also moves planets around during the chaotic period characterized by mutual close encounters between the planets prior to the ejection of one (or more) out of the system.

A planetesimal belt can be affected by the dynamical behaviour of the planets, and we can envision different scenarios in which planets and planetesimal belts interact, evolve and finally coexist. We are interested in a scenario where a planet perturbs the belt from an inside eccentric orbit. This configuration can be achieved via a smooth path where the planet, after its formation, evolved close to the belt without dramatic dynamical events and in a low-eccentricity orbit. In this case, the belt is expected to be initially cold before the onset of the secular perturbations of the planet. If instead the planet is involved in a period of planet–planet scattering, its present location close to the belt would be the outcome of a chaotic past and its eccentricity is expected to be high. In this second scenario, the belt may have been affected by a period of planet–planet scattering at different levels. It may have been spared by most of the chaotic evolution of the planets and, when one planet ends up in a close orbit, be directly affected by its secular perturbations starting from a non-excited state (initial cold belt). In alternative, it may have been stirred up by the planets evolving on highly eccentric orbits induced by the mutual close encounters before a quiet state is established following the ejection of one or more bodies. In this case, a warm belt with excited eccentricities and, possibly, inclinations would interact with the planet that finally ends up in an orbit close to the belt at the end of the chaotic phase. Intermediate states can also be envisioned where the belt is warmed either by self-stirring induced by the formation of large embryos or by resonance sweeping by a migrating planet or other possible mechanisms before being perturbed by an incoming planet.

In this paper, we apply a semi-analytic method specifically designed to compute both $P_{\rm i}$ and $U_{\rm c}$ for belts perturbed by a nearby planet. Its secular perturbations force a strong correlation between the eccentricity e and perihelion longitude ϖ of the planetesimal orbits significantly affecting the values of both $P_{\rm i}$ and $U_{\rm c}$. The knowledge of these two dynamical parameters allows us to model the collisional evolution of a belt and quantitatively predict its erosion over the star age. With suited collisional models these parameters can also be used to infer the early planetesimal population that led to the present belt whose properties are deduced by the related debris disc. From an observational point of view, they can be used to relate the star age to the brightness of the debris disc, taking of course into account the uncertainties on the initial planetesimal population, its physical properties and the planet orbital parameters. It can also predict the frequency of large break-up events in the belt that can lead to a sudden significant enhancement of the brightness of the related debris disc. The parameters we compute can also be used in more refined codes predicting the luminosity of a debris disc for a given planetesimal belt.

We consider distinct dynamical configurations in which the planet perturbs either an initial cold or warm belt. In the case of a warm belt, we also contemplate the case in which there is a significant inclination excitation. In addition, we compute the values of $P_{\rm i}$ and $U_{\rm c}$ for crowded belts where a significant collisional damping may occur. We focus on a standard case with a Jupiter-sized planet orbiting at about 5 au from the star and a planetesimal belt extending beyond 10 au. We show that the secular perturbations of the planet and, in particular, the correlation between e and ϖ typical of these perturbations cause a reduction of both $P_{\rm i}$ and $U_{\rm c}$ with respect to a non-correlated case. This last case may occur, in the absence of a close perturbing planet, if the planetesimal belt self-stirred for example via the formation of large planetary embryos, or if it was perturbed by planets roaming around during a chaotic phase and, when finally a quiet state is reached, it is located far away from any potentially perturbing bodies. This finding suggests that the presence of a perturbing planet not always leads to a higher dust production rate and that self-stirred planetesimal belts might give origin to brighter debris discs. We have tested different values of the planet eccentricity finding higher values of both $P_{\rm i}$ and $U_{\rm c}$ in the presence of more eccentric planets.

We also explore as $P_{\rm i}$ and $U_{\rm c}$ change when a belt was warm before being secularly perturbed by a planet. In this case, the approximation $e_{\rm p} = e_{\rm f}$ cannot be adopted and the proper eccentricity, after the onset of the planet perturbations, can assume a range of values from $e_{\rm f} - e_{\rm p0}$ to $e_{\rm f} + e_{\rm p0}$, where $e_{\rm p0}$ is the average eccentricity of the warm planetesimal belt before the planet begins to perturb it. In our modelling, we assume that $e_{\rm p0}$ is a fixed fraction of the forced eccentricity, an arbitrary choice simply dictated by the need of avoiding a random selection of initial values. We do not consider scenarios where $e_{\rm p0}$ is initially larger than $e_{\rm f}$. For warm belts, we find an increase in the collisional activity with respect to initially cold belts but they are still less collisionally eroded compared to the 'self-stirred' belts, at least until $e_{\rm p0} \leq e_{\rm f}$. A warm belt is then expected to be gradually depleted on shorter time-scales. A dynamically excited belt may also have high inclinations. In this configuration, an increase of the relative velocity and a decrease of the intrinsic

probability of collision are found. However, the two effects do not compensate and the reduction of P_i leads to a lower erosion rate compared to a small body belt with low inclination. This proves the dominating role of P_i in determining the collisional evolution of a minor body population.

We have applied our formalism to model the case of the debris disc detected in HD 38529. The collisional activity in the putative belt hosting the leftover planetesimals is low compared to the standard case we have studied in this paper, and after 4 Gyr of collisional evolution only a low percentage of bodies smaller than 100 km are expected to have been disrupted by collisions. However, the planetesimal belt appears to be more collisionally active compared to that detected around ϵ Eridani. This finding is at odds with the observations of the debris discs around the two stars with that around ϵ Eridani being more dense with respect to that around HD 38529. One possible explanation is that a turbulent dynamical past depleted the belt around HD 38529 reducing the number density of planetesimals.

On the basis of the secular theory, we can envisage the following evolution of the brightness of a debris disc associated with an initially cold belt. At the beginning, when the planet approaches the belt, the dust production rate will slowly increase during the progressive randomization of the pericentre. When the ϖs are still in phase, low impact velocities are expected but at subsequent times the progressively different values of pericentre longitudes will lead to more energetic collisions and a higher dust production rate. The debris disc will become brighter. When the full randomization is reached, from then on the dominant mechanism will be the slow erosion of the planetesimal belt due to mutual collisions and the brightness of the associated debris disc will slowly decrease with time. The rate of luminosity decrease can be estimated on the basis of P_i and U_c that are the basic parameters to determine the collisional evolution of the belt.

The situation appears slightly more complex for an initially warm belt. At the beginning, just after the arrival of the planet, the pericentre evolution quickly leads pseudo-librators to cross the orbits of circulators causing a fast rise in the collisional rate and an increase in the luminosity of the associated debris disc. However, at subsequent time, this initial highly collisional state will develop into a dynamical configuration where the secular perturbations are fully developed and the erosion will follow the same path as in a cold belt even if with different speed due to the higher values of P_i and U_c.

In the presence of a strong collisional damping, like in a very crowded belt, the dynamics is dominated by the pseudo-libration of all planetesimals and the collisional activity is strongly reduced with values of both P_i and U_c significantly smaller with respect to both the cases of cold and warm non-damped belts.

It is clear that, on the basis of the values of P_i and U_c, we can derive different relations between the brightness of a disc and the age of the star, since the erosion of the belt will be faster or slower depending on the orbital parameters of the planet and the dynamical state of the belt at the onset of the secular perturbations.

In this paper, we have focused on the perturbations of a single planet on a planetesimal belt, but systems of multiple giant planets perturbing coexisting belts can be found as well. In this last case, a more complex secular evolution is expected. However, our algorithm for computing P_i and U_c can be easily applied to these systems once the frequencies of perihelion precession of all planets are computed. If the eccentricities of the planets are high, the linear secular theory may be a rough approximation for computing the real frequencies and higher order theories may be needed (Michtchenko & Malhotra 2004; Libert & Henrard 2005). This problem will be faced in a subsequent paper.

Concerning the contribution from mean motion resonances to the collisional evolution of a belt, it can be considered negligible in a configuration where a single planet perturbs a wide belt considering the small resonance width even for highly eccentric planets. Together with secular resonances, mean motion resonances may cause local differences in the brightness of the debris disc associated with the belt but they are not expected to cause significant differences in the overall collisional evolution of wide belts. For narrow belts, a dedicated dynamical exploration may be necessary to evaluate the contribution of resonances.

ACKNOWLEDGEMENTS

We thank an anonymous referee for his/her useful comments and suggestions that helped to significantly improve the paper.

REFERENCES

Benedict G. F. et al., 2006, AJ, 132, 2206
Bonsor A., Raymond S. N., Augereau J.-C., 2013, MNRAS, 433, 2938
Bottke W. F., Nolan M. C., Greenberg R., Kolvoord R. A., 1994, Icarus, 107, 255
Bottke W. F., Broz M., O'Brien D. P., Campo Bagatin A., Morbidelli A., Marchi S., 2002, in Micheln P., DeMeon F. E., Bottken W. F., Jr, eds, Asteroids IV. Univ. Arizona Press, Tucson, p. 701
Bottke W. F., Durda D. D., Nesvorný D., Jedicke R., Morbidelli A., Vokrouhlický D., Levison H., 2005, Icarus, 175, 111
Bryden G. et al., 2009, ApJ, 705, 1226
Butler R. P. et al., 2006, ApJ, 646, 505
Campo Bagatin A., Cellino A., Davis D. R., Farinella P., Paolicchi P., 1994, Planet. Space Sci., 42, 1079
Chambers J. E., Wetherill G. W., 2001, Meteorit. Planet. Sci., 36, 381
Davis D. R., Farinella P., 1997, Icarus, 125, 50
Davis D., Durda D., Marzari F., Campo Bagatin A., Gil-Hutton R., 2002, in Bottke W. F., Jr, Cellino A., Paolicchi P., Binzel R. P., eds, Asteroids III. Univ. Arizona Press, Tucson, p. 545
Dell'Oro A., 2016, MNRAS, in press
Dell'Oro A., Paolicchi P., 1997, Planet. Space Sci., 45, 779
Dell'Oro A., Paolicchi P., 1998, Icarus, 136, 328
Dell'Oro A., Paolicchi F., Marzari P., Dotto E., Vanzani V., 1998, A&A, 339, 272
Dell'Oro A., Marzari F., Paolicchi P., Vanzani V., 2001, A&A, 366, 1053
Everhart E., 1985, in Carusi A., Valsecchi G. B., eds, Astrophysics and Space Science Library. Vol. 115, IAU Colloq. 83: Dynamics of Comets: Their Origin and Evolution. Reidel, Dordrecht, p. 185
Farinella P., Davis D. R., 1992, Icarus, 97, 111
Greaves J. S. et al., 1998, ApJ, 506, L133
Heppenheimer T. A., 1978, A&A, 65, 421
Hillenbrand L. A. et al., 2008, ApJ, 677, 630
Kalas P. et al., 2008, Science, 322, 1345
Kenyon S. J., Bromley B. C., 2004, AJ, 127, 513
Kral Q., Thébault P., Charnoz S., 2013, A&A, 558, A121
Krivov A. V., 2010, Res. Astron. Astrophys., 10, 383
Li A., Lunine J. I., Bendo G. J., 2003, ApJ, 598, L51
Libert A.-S., Henrard J., 2005, Celest. Mech. Dyn. Astron., 93, 187
MacGregor M. A., Wilner D. J., Andrews S. M., Lestrade J.-F., Maddison S., 2015, ApJ, 809, 47
Marzari F., 2014, MNRAS, 444, 1419
Marzari F., Davis D., Vanzani V., 1995, Icarus, 113, 168
Matthews B. C., Krivov A. V., Wyatt M. C., Bryden G., Eiroa C., 2014, Protostars and Planets VI. Univ. Arizona Press, Tucson, p. 521
Meshkat T. et al., 2015, ApJ, 800, 5
Michtchenko T. A., Malhotra R., 2004, Icarus, 168, 237
Moro-Martín A., Wolf S., Malhotra R., 2005, ApJ, 621, 1079

Moro-Martín A. et al., 2007a, ApJ, 658, 1312
Moro-Martín A. et al., 2007b, ApJ, 668, 1165
Murray C. D., Dermott S. F., 1999, Solar System Dynamics, Cambridge Univ. Press, Cambridge
Mustill A. J., Wyatt M. C., 2009, MNRAS, 399, 1403
Öpik E. J., 1951, Proc. R. Ir. Acad. A, 54, 165
Shannon A., Bonsor A., Kral Q., Matthews E., 2016, MNRAS, 462, L116
Sibthorpe B., Ivison R. J., Massey R. J., Roseboom I. G., van der Werf P. P., Matthews B. C., Greaves J. S., 2013, MNRAS, 428, L6
Stewart S. T., Leinhardt Z. M., 2009, ApJ, 691, L133
Stewart G. R., Wetherill G. W., 1988, Icarus, 74, 542
Su K. Y. L., Rieke G. H., 2014, in Booth M., Matthews B. C., Graham J. R., eds, Proc. IAU Symp. 299, Exploring the Formation and Evolution of Planetary Systems. Cambridge Univ. Press, Cambridge, p. 318
Thébault P., 2012, A&A, 537, A65
Thébault P., Marzari F., Scholl H., 2006, Icarus, 183, 193
Trilling D. E. et al., 2008, ApJ, 674, 1086
Wetherill G. W., 1967, J. Geophys. Res., 72, 2429
Whitmire D. P., Matese J. J., Criswell L., Mikkola S., 1998, Icarus, 132, 196
Wyatt M. C., Smith R., Greaves J. S., Beichman C. A., Bryden G., Lisse C. M., 2007, ApJ, 658, 569

This paper has been typeset from a TEX/LATEX file prepared by the author.